Quantum simulation of topologically protected states using directionally unbiased linear-optical multiports

David S. Simon, Casey A. Fitzpatrick, Shuto Osawa, and Alexander V. Sergienko

Phys. Rev. A **96**, 013858 — Published 31 July 2017

DOI: 10.1103/PhysRevA.96.013858

Quantum Simulation of Topologically Protected States Using Directionally-Unbiased Linear Optical Multiports

David S. Simon,[1,2,*] Casey A. Fitzpatrick,[2,†] Shuto Osawa,[2,‡] and Alexander V. Sergienko[2,3,§]

[1] *Dept. of Physics and Astronomy, Stonehill College, 320 Washington Street, Easton, MA 02357*
[2] *Dept. of Electrical and Computer Engineering & Photonics Center, Boston University, 8 Saint Mary's St., Boston, MA 02215, USA*
[3] *Dept. of Physics, Boston University, 590 Commonwealth Ave., Boston, MA 02215, USA*

It is shown that quantum walks on one-dimensional arrays of special linear optical units allow the simulation of discrete-time Hamiltonian systems with distinct topological phases. In particular, a slightly modified version of the Su-Schrieffer-Heeger (SSH) system can be simulated, which exhibits states of nonzero winding number and has topologically-protected boundary states. In the large-system limit this approach uses quadratically fewer resources to carry out quantum simulations than previous linear-optical approaches and can be readily generalized to higher-dimensional systems. The basic optical units that implement this simulation consist of combinations of novel optical multiports that allow photons to reverse direction.

I. INTRODUCTION

The rapidly expanding research activity currently underway on quantum computing [1–4] is ultimately an outgrowth of Richard Feynman's observation that quantum systems are necessary to efficiently simulate other quantum systems [5–7]. The goal of quantum simulation is therefore to find simple quantum systems that can accurately and efficiently simulate specific properties of interest in more complex quantum physical entities.

The behavior of a quantum system arises from interference between multiple solutions of a linear wave equation. This can be seen most clearly in Feynman's path integral formalism [8, 9], where the observable output state is a linear superposition of all allowed intermediate trajectories. In a similar manner, linear-optical systems make use of interference between light waves that arise as solutions to the linear Helmholtz equation. For systems in which particle number is conserved (electrons in a solid, for example), linear optics would therefore seem to be a natural resource to exploit in order to carry out quantum simulations. In particular, photonic quantum walks [10, 11] can produce the complex interference patterns needed for such simulations. Because of the relatively feeble interactions that photons have with their surroundings, many of the complexities associated with other physical implementations of quantum simulations are greatly reduced in an optical setting. In addition, light is not only easy to produce and detect, but it can be tailor-made with a high degree of control over its frequency, polarization, and spatial and temporal profiles. Further, quantum effects are readily visible in optics; for example, photon pairs can be routinely produced with high degrees of entanglement [12–14].

Systems with nontrivial topological behavior arise naturally in the study of solids, as well as in other areas of physics. They lead to wavefunctions with nonzero Chern number or winding number, to topologically protected edge or boundary states, and to phase transitions between distinct topological states (see [15–19] for reviews). Alongside theoretical work and experimental implementation, quantum simulation of these behaviors has also become an active area of current research. For example, simulations have been carried out with ultracold atoms, both in free space and confined to optical lattices [20–26], as well as in photonic quantum walks [16, 27–30].

The approaches used up to now for quantum simulations of topologically-nontrivial physical systems have substantial limitations. For example, working with atoms requires extremely low temperatures in order to avoid decoherence. This adds numerous complications to the experiments and makes this approach unlikely to be useful outside of research labs. On the other hand, analogous simulations done with optical quantum walks have their own complications. In particular, they require a set of optical resources (beam splitters, mirrors, etc.) that grows rapidly with the number of steps in the walk.

These factors strongly limit the ability to use the current optical approaches for practical simulations on a large scale, and so it is of interest to investigate novel schemes that may be more easily scalable. Here we present a linear-optical strategy whose resource requirements grow at a quadratically slower rate than previous optical approaches. It is currently practical to carry out a table-top version of this procedure, and in the near future it should be plausible to implement it on much larger scales by integrating all of the required optical elements onto optical chips that can be fabricated in large numbers and arranged into the desired configurations with high stability. In contrast to the quadratic growth in previous optical implementations, the resources required here scale only linearly with number of steps. Furthermore, this scheme has the advantage that the parameters of the underlying system on which the walk occurs can

*e-mail: simond@bu.edu
†e-mail: cfitz@bu.edu
‡e-mail: sosawa@bu.edu
§e-mail: alexserg@bu.edu

be readily varied to produce a variety of simulated behaviors.

In [31] a linear-optical method was proposed for using photonic quantum walks to carry out quantum simulations of topologically-trivial nearest-neighbor Hamiltonians in the context of one-dimensional discrete-time physical models. This was accomplished by means of chains of simple linear optical units. Different Hamiltonians could be simulated by varying the arrangement of these units, or by varying their internal parameters. By going from a one-dimensional chain to two- or three-dimensional arrays, Hamiltonians exhibiting more complicated band gap structures can also be implemented.

In the current paper, the simple periodic lattice of [31] is replaced by a pair of two interlaced sublattices with different parameters, leading to a substantial generalization in the types of behaviors attainable. In particular, simulation of topologically non-trivial Hamiltonians become possible, with features such as nonzero winding number and topologically-protected boundary states.

The basic optical units utilized in this scheme are the directionally-unbiased optical multiports proposed in [32]. These devices can be thought of as scattering centers of the type that have been discussed in the abstract context of optical graph systems [33–36]. In a graph model, an incident photon is constrained at each time step to scatter into one of a finite number of modes. One of these modes is the time-reversed version of the input mode, so it is necessary that the multiport allows the photon to reverse direction and exit back out the input port. Such reversible multiports can be constructed using only linear optics and can be thought of as artificially-created optical "meta-atoms", with lattices of them forming a type of metamaterial. In this sense, the current paper is complementary to work that seeks to produce topological behavior in dielectric metamaterials [37].

The significant reduction in resources in the current proposal compared to previous optical approaches is a direct consequence of the fact that the input ports of the unbiased multiport serve also as output ports. As a result, the flow of photons can reverse direction and traverse the same unit multiple times instead of needing additional units at each time step. This is illustrated in Figure 1: previous linear-optical implementations involve a splitting of optical paths at each step, causing the number of outputs and the number of beam splitters, phase plates, etc. to increase with each step. Although the overall flow of photons in time is toward right, the quantum walk is occurring in the transverse direction. If N is the number of time steps, then the total resources grow proportional to N^2. Effectively, the standard approach requires a two-dimensional network to carry out a one-dimensional walk. However, with reversible units of the type used in the current paper, the walk occurs in the longitudinal (horizontal) direction, requiring only a single line with length of order N to carry out a walk of N steps. The currently-proposed method also scales up to systems with more spatial or internal degrees of freedom in a straightforward manner.

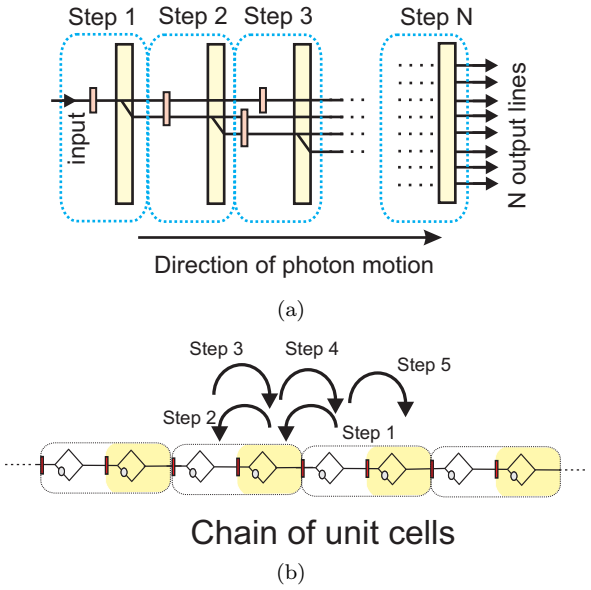

FIG. 1: (a) In prior approaches to topological system simulation with linear optics, the number of optical lines increases with each step and the walk occurs in the transverse direction, requiring quadratic increase of resources as the number of steps increases. (b) The approach using directionally-unbiased multi-ports only requires motion along a single line to produce the same effect. The quantum walk is in the longitudinal, rather than the transverse direction, and so only requires linear resource growth.

We briefly review directionally-unbiased multiports and topologically non-trivial discrete-time Hamiltonian systems in Sections II and III, respectively, before using the multiports to demonstrate linear optical simulation of topologically protected states in section IV. We briefly discuss these results in section V.

II. DIRECTIONALLY-UNBIASED MULTIPORTS

Ordinary beam splitters and their multiport generalizations only allow one-way movement of photons; the light never reverses direction inside. In [32], a generalized multiport was proposed which allows such a reversal. Such a device, called a directionally unbiased multiport, allows the experimental implementation of scattering-based quantum walks on graphs [34–36]. Examples of unbiased n-ports for $n = 3$ and $n = 4$ are shown in Fig. 2(a) and (b). Only the three-port version will be used in the following.

The directionally unbiased multiports are linear optical devices with the input/output ports attached to vertex units of the form shown in the inset of Fig. 2(a). Each such unit contains a beam splitter, mirror and phase shifter. The beam splitter-to-mirror distance $\frac{d}{2}$ is half of

the distance d between the vertex units in the multiport. The phase shifter provides control of the properties of the multiport, since different choices of phase shift at the vertices affect how the different photon paths through the device interfere with each other.

If the unit is sufficiently small (quantitative estimates of the required size and other parameter values may be found in [32]) then its action can be described by an $n \times n$ unitary transition matrix $\hat{U}$ whose rows and columns correspond to the input and output states at the ports. If the internal phase shifts at all three mirror units are equal, then an explicit form of the unitary transition matrix $\hat{U}$ can be found:

$$\hat{U} = \frac{e^{i\theta}}{2 + ie^{i\theta}} \begin{pmatrix} 1 & ie^{-i\theta} - 1 & ie^{-i\theta} - 1 \\ ie^{-i\theta} - 1 & 1 & ie^{-i\theta} - 1 \\ ie^{-i\theta} - 1 & ie^{-i\theta} - 1 & 1 \end{pmatrix}, \quad (1)$$

where θ is the total phase shift at each mirror unit (including both the mirror and the phase plate). The rows and columns refer to the three ports A, B, C.

Two special cases of this result can be noted. First, if the internal phase shifts at the vertices are set to $\theta = \frac{\pi}{6}$ then the exit probabilities at all three ports are equal, but at the cost of having different phase factors for different transitions. The case where are all the exit probabilities are equal is referred to as the *strictly unbiased* case [31].

A second notable special case of Eq. 1 is when $\theta = -\frac{\pi}{2}$. This choice ensures that all of the photon paths entering and exiting at any pair of ports will be in phase with each other [32]. The transition amplitude is then always pure imaginary for every pair of input and output ports, which provides simplifications when adding multiple transition amplitudes. For this case, which will be the main focus here, the three-port takes an input state $|\psi_0\rangle$ to an output state $|\psi\rangle = \hat{U}|\psi_0\rangle$, where

$$\hat{U} = -\frac{i}{3} \begin{pmatrix} 1 & -2 & -2 \\ -2 & 1 & -2 \\ -2 & -2 & 1 \end{pmatrix}. \quad (2)$$

The simulation system of section IV will be built from units described by Eq. 2.

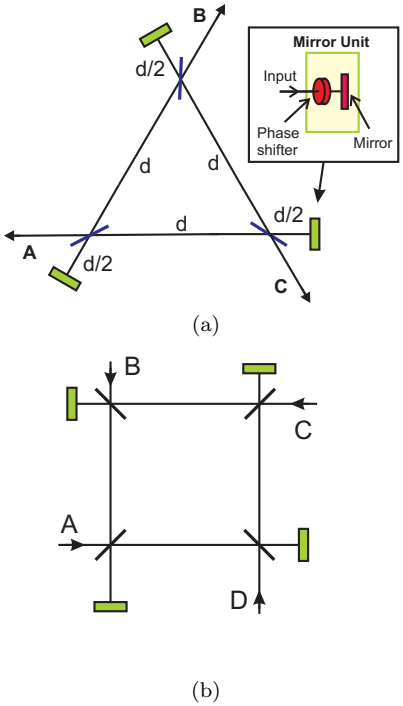

FIG. 2: (a) The directionally-unbiased three-port. (b) The directionally-unbiased four-port. The rectangles after the beam splitters in (a) and (b) represent the vertex mirror unit shown in the inset of (a). This unit consists of a mirror and a phase-shifter. The distance between each beam splitter and the adjacent mirror unit is half the distance d between one beam splitter and the next.

III. WINDING NUMBERS AND TOPOLOGICALLY PROTECTED STATES

A. Topological phases

The object of study here is a discrete time system, described by a Hamiltonian $\hat{H}$ and a discrete-time evolution matrix $\hat{U} = e^{-i\hat{H}T}$ that takes the system forward one time-step T. (Here, the units are chosen such that $\hbar = 1$.) For initial state $|\psi(0)\rangle$, the state at time $t = nT$ is

$$|\psi(nT)\rangle = \hat{U}^n|\psi(0)\rangle. \quad (3)$$

Wedging the matrix $\hat{U}$ between a pair of desired initial and final states gives the transition amplitude per time step between those states. We define quasi-momentum k on a one-dimensional periodic lattice made from a sequence of repeating unit cells. These cells are labeled by an integer, m. Since the position variable m is dimensionless and discrete, the quasi-momentum k will be as well. A single Brillouin zone runs from 0 to 2π, and k is only conserved modulo 2π.

The Hamiltonian generates time evolution in some space that may include both spatial and internal degrees of freedom. As the momentum is varied over the width of a full Brillouin zone, the parameters defining $\hat{H}$ will trace out a closed path in the parameter space. Topological obstructions may prevent some of these paths from being continuously deformed into each other as the system parameters vary, leading to distinct topological phases of the system. In this case, all quantities that are constant on each equivalence class will be topologically protected and stable under small perturbations. The distinct phases are usually distinguished by integer-valued quantities such as the the winding number ν in one-dimensional lattice systems or the Chern number two-dimensions.

When two one-dimensional systems with different

topological phases are brought into contact, solutions can only propagate from one region to the other if they change winding number, which in turn only occurs if the band gap between quasi-energy levels vanish at the boundary. The closing of the gap therefore implies the existence of states that are exponentially localized in the vicinity of the boundary [16, 17], and continuous variations of the system parameters in the two bulk regions leave them intact. These boundary states have been widely studied in recent years [41–44].

B. The SSH model.

An example of a Hamiltonian with topological states is the Su-Schreiffer-Heeger (SSH) Hamiltonian [39], which is used, for instance, to model the hopping of electrons along the length of a polyacetylene chain, and which is closely related to a structure appearing in quantum field theory models [40].

The SSH system is shown schematically in Fig. 3. There is a set of lattice sites or cells (labeled by integer m), each of which contains two subsites, denoted as a and b in the figure; these two lattice subsites represent possible "internal" states at cell m. There is some amplitude per unit time v to switch between the two states within the same cell, and an amplitude per time w to hop to the adjacent lattice sites. When the site changes, the state also flips, and the amplitudes have to be symmetric in the sense that they are the same (up to complex conjugation) for hops to the left and to the right.

The Hamiltonian is of the form:

$$\begin{aligned}\hat{H} &= v\sum_{m=1}^{N}\left(|m,b\rangle\langle m,a| + |m,a\rangle\langle m,b|\right) \\ &\quad + w\sum_{m=1}^{N-1}\left(|m+1,a\rangle\langle m,b| + |m,b\rangle\langle m+1,a|\right),\end{aligned} \tag{4}$$

where N is the number of cells in the chain. $|m,a\rangle$, for example, denotes the state with a particle at site m in substate a.

At each fixed lattice site m or each fixed k, this Hamiltonian is therefore a two-dimensional matrix, and can be written in terms of the identity matrix and the Pauli matrices; for example, in momentum space one may write

$$\hat{H}(k) = d_0(k)I + \boldsymbol{d}(k)\cdot\boldsymbol{\sigma}. \tag{5}$$

This describes dynamics in a two dimensional "internal" subspace labeled by the two substates present at each lattice site. Generically, the two energy levels are separated by a k-dependent gap.

The insulator described by this Hamiltonian becomes a conductor when the vector $\boldsymbol{d}(k)$ vanishes; at these points the discrete energy levels meet and the energy gap between bands vanishes. In the SSH model $d_0 = d_z = 0$, so that the space of possible $\boldsymbol{d}$ values collapses to the two-dimensional (d_x, d_y) plane. This means that paths encircling the origin cannot be contracted continuously to a point and have nonzero winding number. The winding number is highly stable in the sense that perturbations causing continuous variations of the parameters cannot stimulate transitions between topological classes. The SSH system therefore can support highly localized boundary states at the interfaces between regions of different topological phase. The appearance of such localized states will be used in the next section as a signal to verify the existence of distinct topological phases.

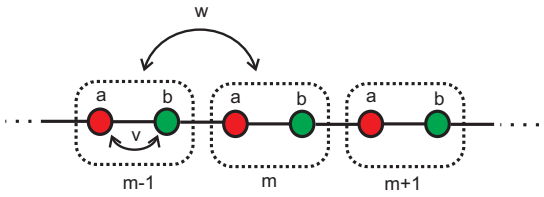

FIG. 3: The SSH Hamiltonian describes motion of a particle hopping on a chain of sites with two substates per site. v and w are respectively the intracell and intercell hopping amplitudes per unit time.

IV. SIMULATING THE MODIFIED SSH HAMILTONIAN OPTICALLY

It was shown in Ref. [32] that the unbiased multiport described by Eq. 2 provides a physical realization of the abstract three-point scattering vertex used in several studies of quantum walks on graphs [34–36]. We now take advantage of that equivalence in order to apply some of those graph-based results to a physically implementable optical system. In particular, the basic building blocks of the system will be the units shown on the left in Fig. 4, whose properties were studied in [34–36]. Each such diamond graph consists of a pair of three-point scattering vertices connected at two edges, with an additional phase shift on one connecting edge. The remaining two edges provide input/output lines. Given the equivalence between the scattering centers and the unbiased three-ports, this system can be physically implemented by a pair of unbiased three-ports, as shown on the right in Fig. 4, with each graph edge corresponding to an allowed optical path. It is assumed here that the multiports are very small (effectively pointlike) compared to the distance d between them.

To simulate SSH-like behavior, each a and b subsite in Fig. 3 is formed from one such diamond graph, so each unit cell contains four multiports and two phase shifters. The phase shifts ϕ_a and ϕ_b in the two diamonds may be different from each other; they are adjustable parameters that can be varied independently.

Drawing the simulation system in the form of the abstract diamond graphs, it then looks as shown in Fig. 5. The red rectangles are phase plates, rotating the polar-

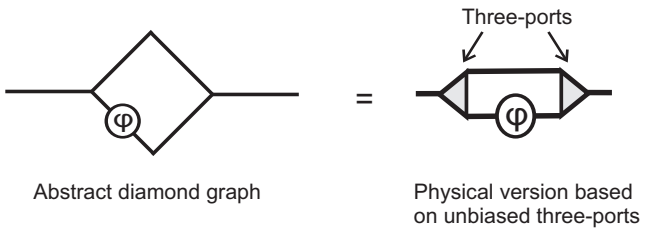

FIG. 4: The abstract diamond graph [34–36] consists of two three-port scattering vertices connected on two edges, with a phase shift between them (left). Since the scattering vertices can be implemented physically by unbiased three-ports, the diamond graph is equivalent to a pair of directionally unbiased three-ports arranged as shown on the right.

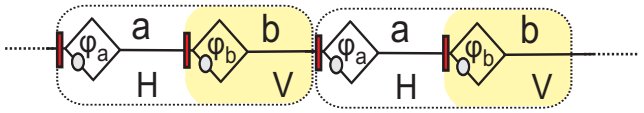

FIG. 5: Simulating the SSH Hamiltonian with diamond graphs. Each graph is made from two directionally unbiased three-ports, as shown in Fig. 4, so that each cell (indicated by the dashed curves) is made from four three-ports. The two diamond graphs at each site may have different internal phase shifts, ϕ_a and ϕ_b. The red rectangles are phase plates that rotate the polarization by 90°, so photons in the shaded areas have vertical polarization (state b), while the unshaded regions have horizontal polarization (state a). The size of the diamond graphs is exaggerated for clarity: they should be small compared to the distance separating them.

ization by 90°. The time unit T is taken to be the time to go from one diamond graph to the next, or equivalently from one phase plate to another. Having a photon present in the areas labeled a and b, bounded by the phase plates, represent the two substates at each lattice site. If $\phi_a \neq \phi_b$, the two triangle graphs inside each cell will have different transmittances. Let $T_a = |t_a|^2$ and $T_b = |t_b|^2$ then be the transmission probabilities corresponding to the two graphs. In order to make it easy to measure which subsite the photon is in within a cell, the phase plates will flip the polarization each time the substate changes. Here, the polarization simply serves as a convenient bookkeeping device to make experimental distinguishability of the a and b states easier, and is not essential to the theoretical development. Photons can be easily coupled in and out of the system by means of optical switches and optical circulators as described in more detail in [31].

There is one photon collision with a diamond graph per unit time. At each encounter with one of these graphs, there are amplitudes to either reflect back from it into the original subsite, or to be transmitted through to an adjacent subcell. The hopping amplitudes v and w are then given by the transmission amplitudes of the diamond graphs. Without loss of generality, an appropriate redefinition of states may always be used to make the amplitudes real, in which case

$$\langle m,a|m,b\rangle = |t_a| \tag{6}$$

$$\langle m+1,a|m,b\rangle = \langle m,b|m+1,a\rangle = |t_b|. \tag{7}$$

Transitions in which the photon reflects off the diamond graph and back into the same subcell give diagonal contributions to the Hamiltonian that simply shift all of the energies up or down by the same amount; i.e. they define the zero level of the energy. These terms can therefore be ignored for current purposes. The remaining terms are those that take a photon from one subcell to an adjacent subcell in a single time step; in other words, terms of the form that appear in the Hamiltonian of 4. The hopping amplitudes v and w between subcells are given by the transmission coefficients of the diamond graphs. Therefore, the Hamiltonian of interest is

$$\hat{H} = |t_a| \sum_{m=1}^{N} (|m,b\rangle\langle m,a| + |m,a\rangle\langle m,b|) + |t_b| \sum_{m=1}^{N-1} (|m+1,a\rangle\langle m,b| + |m,b\rangle\langle m+1,a|), \tag{8}$$

where the diamond graph transmission amplitudes for phase shifts are [34–36]:

$$t_j(k) = \frac{4(1+e^{-i\phi_j})(1-e^{-i(\phi_j+4k)})}{e^{-4ik}(1+e^{-i\phi_j})^2 - (3e^{-i(\phi_j+4k)}-1)^2}, \tag{9}$$

where $j = a, b$.

A. Quasi-energies and transmission amplitudes.

It is convenient to work in quasi-momentum space. Carrying out the Fourier transform,

$$|k\rangle = \frac{1}{\sqrt{N}} \sum_{m=1}^{N} e^{imk}|m\rangle, \tag{10}$$

the momentum-space Hamiltonian is then a matrix in the a-b internal space:

$$\hat{H} = \frac{1}{N} \sum_{k} \hat{H}(k)\ |k\rangle\langle k|, \tag{11}$$

where

$$\hat{H}(k) = \langle k|\hat{H}|k\rangle = \frac{1}{N} \begin{pmatrix} 0 & |t_a| + |t_b|e^{-ik} \\ |t_a| + |t_b|e^{ik} & 0 \end{pmatrix}. \tag{12}$$

For each value of k, this has two eigenvalues

$$E_{\pm}(k) = \pm\sqrt{|t_a|^2 + |t_b|^2 + 2|t_a t_b|\cos k}. \tag{13}$$

Plotting E versus k gives the analog of a band-gap diagram with minimum band gap Δ. When v and w

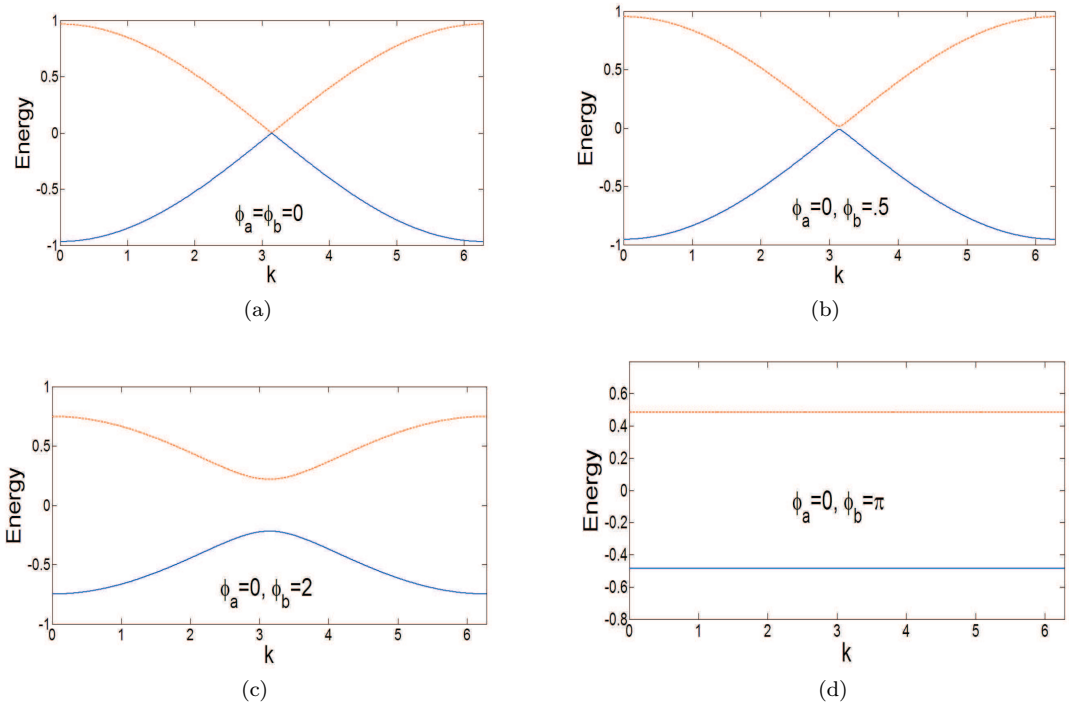

FIG. 6: Energy bands for the system shown in Fig. 5. The band gap vanishes when the two phases are equal (a) and opens up when the two phase values differ. The gap is still very small in (b), but grows as $|\phi_a - \phi_b|$ increases (c), reaching its maximum size when $|\phi_a - \phi_b| = \pi$ (d).

are independent of k, as in the usual SSH case, then $\Delta = 2|v - w|$, but notice that in the present case v and w depend on momentum via the k-dependent transmittances. In this sense, this is not the true SSH model, but a slight variant of it, which we might call the modified SSH (MSSH) model; this is a continuous deformation of the usual SSH model and so should have topologically identical behavior, as will be verified below.

The nonvanishing coefficients of the Pauli matrices in Eq. 5 are now

$$d_x(k) = |t_a(k)| + |t_b(k)| \cos k \quad (14)$$
$$d_y(k) = |t_b(k)| \sin k. \quad (15)$$

As k goes from 0 to 2π, $\boldsymbol{d}$ traces out paths labeled by their winding numbers ν about the origin. These winding numbers will be functions of the hopping amplitudes: $\nu(v, w) = \nu(|t_a|, |t_b|)$. Since t_a and t_b vary only weakly with k, it is clear that the loop traced out by $\boldsymbol{d}(k)$ encloses the origin and has nonzero winding number if $|t_b| > |t_a|$.

B. Verifying topological behavior: localized boundary states.

Properties of the system of Fig. 5 can be numerically simulated, and the results verify that the model constructed here has behavior similar to that expected from the SSH model. Fig. 6 shows plots of the energy levels for different values of the phase shifts ϕ_a and ϕ_b of the two graphs. When the two phase shifts are equal, the band gap vanishes. As they begin to differ, a gap opens up and becomes larger with increasing $|\phi_a - \phi_b|$, reaching a maximum at $|\phi_a - \phi_b| = \pi$, as Fig. 6 shows. The exact shapes of the curves are slightly different than the pure SSH model (in particular, the value of k that minimizes the gap clearly shifts horizontally as the parameter changes), but the qualitative behavior is identical.

Similarly, it is easy to show that different values of the phase shifts allow solutions with both zero and nonzero winding numbers to occur. Evaluation of Eqs. 9, 14, and 15 for a range of ϕ_a and ϕ_b values readily shows that varying these phases causes the path traced out by $\boldsymbol{d}$ to shift horizontally and change radius, leading to transitions between winding numbers 0 and 1. This indicates that different phase values in the two diamond graphs lead to different topological phases, distinguished by their winding numbers. By attaching two chains of these graphs with different winding numbers on each chain there should then arise localized, topologically-protected states at the boundaries between them [15–17].

Fig. 7 supports this analysis by showing specific conditions under which topologically protected states can be generated using a network of multiports. The plots compare two numerical simulations of a single photon quantum walk on the MSSH model described above for

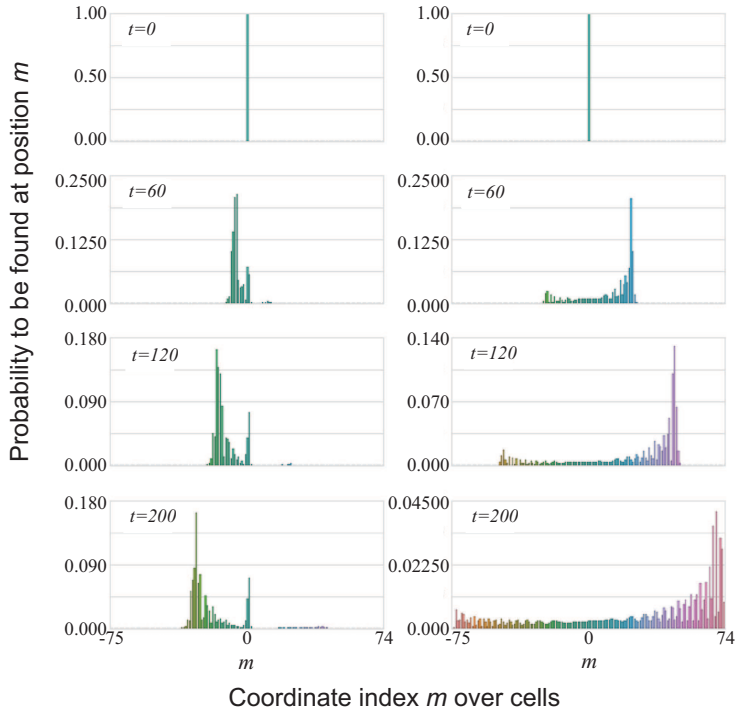

FIG. 7: Comparison of MSSH quantum walk with topologically protected edge state (left) and MSSH quantum walk with normal ballistic spreading (right) for $0 \leq t \leq 200$. The two walks are simulated for the arrangement shown in Fig. 5. The topology on the left uses $(\phi_a = 1.5, \phi_b = 2.5)$ when $m \leq 0$, giving a winding number $\nu \neq 0$; this joins up with a $\nu = 0$ region having phase shifts of $(\phi_a = 3\pi/4, \phi_b = 0)$ when $m \geq 0$. The result is a localized state confined to the boundary of these topologies, indicated by the peak that arises at $m = 0$. In contrast, the topology on the right uses $\phi_a = 0, \phi_b = 0$ for all m, leading to a ballistic quantum walk in one dimension.

$0 \leq t \leq 200$ in units of T. In each case an initially right-moving photon is injected at subsite a of the $m = 0$ position coordinate at $t = 0$ (top row). (The mechanism for physically inserting photon states into the chain is described in detail in Ref. [31].) The left hand column shows the time evolution over a chain with two different topologies attached to each other at $m = 0$. The right hand side shows time evolution over a chain with uniform topology.

Specifically, the left column of Fig. 7 uses subsite phase shifts of $\phi_a = 1.5, \phi_b = 2.5$ for the portion to the left of the origin ($m \leq 0$), giving a winding number $\nu \neq 0$ in that region. To the right of the origin ($m \geq 0$), phase shifts of $\phi_a = 3\pi/4, \phi_b = 0$ are used, giving $\nu = 0$. The result is a persistent probability of finding the photon at the boundary between the two topologies, the signature of a topologically protected edge state [16].

For comparison, the right column of Fig. 7 shows a quantum walk over the MSSH model using no change in phase shifts: $\phi_a = 0, \phi_b = 0$ for all m (positive and negative). As expected, in this case evolution reduces to a standard quantum walk in one dimension, exhibiting ballistic spreading of probability over the coordinates.

Note that the right side of Fig. 7 is asymmetric. This is because the value $\phi_a = \phi_b$ that was used reduces the lattice to a chain of three-ports with transition matrix of form Eq. 2; this matrix has much smaller amplitude to reflect out the input port than to transmit out the other two, resulting in a strong bias of the photon to continue moving in its initial direction. For other values of ϕ_a or ϕ_b (or for other values of the internal vertex phase θ of Eq. 1) this bias changes or disappears.

It may also be pointed out that the diamond graphs have four bound states [35] when $\phi_a - \phi_b = 0$, and none for $\phi_a - \phi_b \neq 0$. These bound states occur in all the diamond graphs at exactly at the parameter values $\phi_a = \phi_b = 0$ at which the energy gap closes. This allows the controlled storage of photons: photons can be stored in the graph or released as the value of ϕ is changed.

V. CONCLUSIONS

Systems with distinct topological phases are of increasing importance in condensed matter physics and in quantum computing. The ability to simulate their properties

in a simple manner is therefore of current interest, and the ability to supply such simulations efficiently using only linear optical quantum systems would be a useful advance. Here, a method for simulation of systems in the same topological class as the SSH Hamiltonian was proposed that for large numbers of time steps requires substantially fewer resources than the method of [30].

In this paper the focus was on the use of only one-dimensional chains of directionally-unbiased optical three-ports. However, this only scratches the surface of the possibilities to be examined, since the current approach can be generalized to two- and three-dimensional arrays of n-ports with $n > 3$. The phase shifts at each vertex of the multiport can also be varied, altering the multiport properties. Thus a rich array of more sophisticated simulation types remains as-yet unexplored, using the same general methods. These hold promise to provide quantum simulation of a diverse range of further phenomena.

Acknowledgements

This research was supported by the National Science Foundation EFRI-ACQUIRE Grant No. ECCS-1640968, NSF Grant No. ECCS- 1309209, and by the Northrop Grumman NG Next.

[1] M. A. Nielsen and I. L. Chuang, *Quantum Computation and Quantum Information* (Cambridge Univ. Press, Cambridge, 2001).
[2] K. A. Yu, A. H. Shen,and M. N. Vyalyi M N, *Classical and Quantum Computation* (American Mathematical Society, Providence, 2002).
[3] G. Jaeger, *Quantum Information: An Overview* (Springer, Berlin, 2006).
[4] G. Falci and E. Paladino, *Int. J. Quant. Inf.* **12**, 1430003 (2014).
[5] R. P. Feynman, *Int. J. Theor. Phys.* **21** 467 (1982).
[6] A. Aspuru-Guzi and P. Walther, *Nat. Phys.* **8**, 285 (2012).
[7] T. H. Johnson, S. R. Clark and D. Jaksch, *EPJ Quantum Technology* **1**, 10 (2014).
[8] R. P. Feynman, *Rev. Mod. Phys.* **20**, 367 (1948).
[9] R. P. Feynman, A. R. Hibbs, D. F. Styer, *Quantum Mechanics and Path Integrals* (Dover, Mineola, NY, 2010).
[10] J. Kempe, *Contemp. Phys.* **44**, 307 (2003).
[11] S. E. Venegas-Andraca, *Quant. Inf Proc.* **11**, 1015 (2012).
[12] Y. Shih, *Rep. Prog. Phys.* **66**, 1009 (2003).
[13] Z. Y. J. Ou, *Multi-Photon Quantum Interference* (Springer, Berlin, 2007).
[14] D. S. Simon, G. Jaeger, A. V. Sergienko, *Quantum Metrology, Imaging, and Communication* (Springer, Berlin, 2017).
[15] M. Z. Hasan and C. L. Kane, *Rev. Mod. Phys.* **82**, 3045 (2010).
[16] T. Kitagawa, *Quant. Inf. Proc.* **11**, 1107 (2012).
[17] J. K. Asbóth, L. Oroszlány, and A. Pályi, *A Short Course on Topological Insulators* (Springer, Berlin, 2016).
[18] B. A. Bernevig, T. L. Hughes, Topological Insulators and Topological Superconductors (Princeton University Press, Princeton, 2013).
[19] T. D. Stanescu, *Introduction to Topological Matter and Quantum Computation* (CRC Press, Boca Raton, 2017).
[20] J. Ruostekoski, G. V. Dunne, and J. Javanainen, Phys. Rev. Lett. **88**, 180401 (2002).
[21] J. Ruostekoski, J. Javanainen, and G. V. Dunne, Phys. Rev. A **77**, 013603 (2008).
[22] X.-J. Liu, Z.-X. Liu, andM. Cheng, Phys. Rev. Lett. 110, 076401 (2013).
[23] X. Li, E. Zhao, and W. V. Liu, Nat. Commun. **4**, 1523 (2013).
[24] J. Javanainen and J. Ruostekoski, Phys. Rev. Lett. **91**, 150404 (2003).
[25] D.-W. Zhang, L.-B. Shao, Z.-Y. Xue, H. Yan, Z. D. Wang, and S.-L. Zhu, Phys. Rev. A **86**, 063616 (2012).
[26] D.-W. Zhang, F. Mei, Z.-Y. Xue, S.-L Zhu, and Z. D. WangPhys. Rev. A **92**, 013612 (2015).
[27] M. A. Broome, A. Fedrizzi, B. P. Lanyon, I. Kassal I, A. Aspuru-Guzik, and A. G. White,*Phys. Rev. Lett.* **104**, 153602 (2010).
[28] T. Kitagawa, M. S. Rudner, E. Berg, and E. Demler *Phys. Rev. A* **82**, 033429 (2010).
[29] T. Kitagawa, E. Berg, M. Rudner, and E. Demler, *Phys. Rev. B.* **82**, 235114 (2010).
[30] T. Kitagawa, M. A. Broome, A. Fedrizzi, M. S. Rudner, E. Berg, I. Kassal, A. Aspuru-Guzik, E. Demler, A. G. White, *Nature Comm.* **3**, 882 (2012).
[31] D. S. Simon, C. A. Fitzpatrick, S. Osawa, and A. V. Sergienko, *Phys. Rev. A* **95** 042109 (2017).
[32] D. S. Simon, C. A. Fitzpatrick and A. V. Sergienko, *Phys. Rev. A* **93**, 043845 (2016).
[33] M. Hillery, J. Bergou, and E. Feldman,*Phy. Rev. A* **68** 032314 (2003).
[34] E. Feldman and M. Hillery, *Phy. Lett. A*, **324** 277 (2004).
[35] E. Feldman and M. Hillery, *Cont. Math.*, **381** 71 (2005).
[36] E. Feldman and M. Hillery, *J. Phys. A: Math. Theor.* **40**, 11343 (2007).
[37] A. Slobozhanyuk, S. H. Mousavi, X. Ni, D. Smirnova, Y. S. Kivshar, A. B. Khanikaev, *Nat. Phot.* **11**, 130 2016.
[38] I. Carneiro, M. Loo, X. Xu, M. Girerd, V. Kendon and P. L. Knight, *New J. Phys.* **7**, 156 (2005).
[39] W. P. Su, J. R. Schrieffer, and A. J. Heeger, *Phys. Rev. B* **22**, 2099 (1980).
[40] R. Jackiw and C. Rebbi, *Phys. Rev. D* **13**, 3398 (1976).
[41] H. Obuse and N. Kawakami, Phys. Rev. B **84**, 195139 (2011).
[42] J. K. Asbóth, Phys. Rev. B **86**, 195414 (2012).
[43] J. K. Asbóth and H. Obuse, Phys. Rev. B **88**, 121406 (2013).
[44] J. K. Asbóth and J. M. Edge, Phys. Rev. A **91**, 022324 (2015).